Chapter 5

Numerical Investigation of the Influence of Steam Addition, Gasification Reactions and NO_x Emission Under Oxy-Coal Combustion

5.1 Overview

In this chapter, numerical investigation of the influence of higher concentration steam addition on oxy-coal combustion process has been studied as the burning of pulverized coal particle takes place under enriched steam conditions under practical combustion cases. Steam has been added by 10-50% to obtain various wet oxy-coal combustion cases. Comparison between ideal dry recycle oxy-coal combustion case with wet oxy-coal combustion cases (10-50% H_2O), and oxy-steam combustion case (H_2O replaces CO_2 in the oxidizer) has been presented. Influence of gasification reactions on temperature profile and species concentration has also been assessed employing the developed numerical model. Furthermore, the computation of NO_x emission under oxy-coal combustion atmosphere has been presented in this chapter. Influence of discussed important operating parameters on NO_x concentration distribution inside the combustion chamber has been calculated by post-processing.

5.2 Influence of Steam Addition

In this section, the influence of steam addition in the oxidizer on the resulting reactive flow field and combustion characteristics have been investigated. A comparison of dry recycle oxy-coal combustion case (0% H_2O) with the different wet oxy-coal combustion cases (10-50% H_2O) and oxy-steam combustion (H_2O replaces the whole CO_2 of the oxidizer) has also been presented in this section. The operating conditions of various oxy-coal combustion cases obtained by varying the steam concentration of the oxidizer are provided in Table 5.1. The operating conditions of various oxy-coal combustion cases are derived on the basis of identical flow field distribution.

Table 5.1 Operating conditions of various oxy-coal combustion cases

Parameter	**Combustion case**						
	0% Steam	**10% Steam**	**20% Steam**	**30% Steam**	**40% Steam**	**50% Steam**	**Oxy-steam**
Coal mass flow rate (kg/s)	0.0018	0.0018	0.0018	0.0018	0.0018	0.0018	0.0018
Primary stream flow rate (kg/s)	0.00486	0.00455	0.004251	0.003947	0.003642	0.003338	0.00245
Secondary stream flow rate (kg/s)	0.00740	0.00694	0.006478	0.006014	0.00555	0.005086	0.00374
Tertiary stream flow rate (kg/s)	0.000416	0.00039	0.000364	0.000338	0.000312	0.000286	0.00021
Staging stream flow rate (kg/s)	0.01525	0.01429	0.01333	0.01328	0.01142	0.01047	0.00770
$O_2/CO_2/H_2O$ [vol%] /[vol%]	21/79/0	21/69/10	21/59/20	21/49/30	21/39/40	21/29/50	21/0/79

5.2.1 Flow Field and Temperature Distribution

The axial velocity contours of various oxy-coal combustion cases having steam content from 0-50% in oxidizer and oxy-steam combustion case (H_2O replaces the whole CO_2 in the oxidizer) are shown in Fig. 5.1. Combustion cases considered in the study have almost similar axial velocity profile. All combustion cases have an internal recirculation zone near the axis of the furnace and external recirculation zone at 0.1 m radial position from the axis of furnace. With an increase in H_2O concentration, the internal recirculation zone (IRZ) slightly shrinks towards the burner quarl. We have provided quantitative analysis of length internal recirculation zone in Fig. 5.5 (a).

The axial variation of axial velocity for oxy-coal combustion cases (having 0-50% H_2O in the oxidizer) and oxy-steam combustion case (H_2O replaces CO_2 in the oxidizer) is shown in Fig. 5.2. The peak axial velocity slightly increases with an increase in H_2O content in the oxidizer. The highest and lowest peak of axial velocity has been observed for oxy-steam combustion case and 0% H_2O oxy-coal combustion case, respectively. All the oxy-coal combustion cases (0-50% H_2O in the oxidizer) have identical axial velocity profile beyond axial location 0.06 m from the burner exit. Oxy-steam combustion case has a slightly lower value of axial velocity than the oxy-coal combustion cases for the axial locations beyond 0.6 m from the burner.

The temperature contours of oxy-coal combustion cases (having 0-50% H_2O in the oxidizer) and oxy-steam combustion case (H_2O replaces CO_2 in the oxidizer) is shown in Fig. 5.3. The downstream of the combustion chamber has an insignificant influence of variation of oxidizer composition; hence region close to the burner is shown. From the

contour, it can be observed that the extent of the higher temperature zone prolonged with increasing steam content for a specified volume concentration of oxygen. Increasing steam content in oxidizer would result in reduced gaseous volume heat capacity due to the lesser volume heat capacity of steam than CO_2, which is the primary cause of increasing flame temperature under enriched steam oxy-coal combustion cases. Steam has faster oxygen diffusion rate than CO_2. The combined effect of lower volume heat capacity and faster oxygen diffusion rate will enhance the char consumption by gasification reactions under steam rich combustion conditions. A considerable change in flame shape can also be seen from the contour with increasing steam content. The radial distribution of flame gets suppressed with increasing steam content. Oxy-steam combustion case has the largest higher temperature region among other combustion cases.

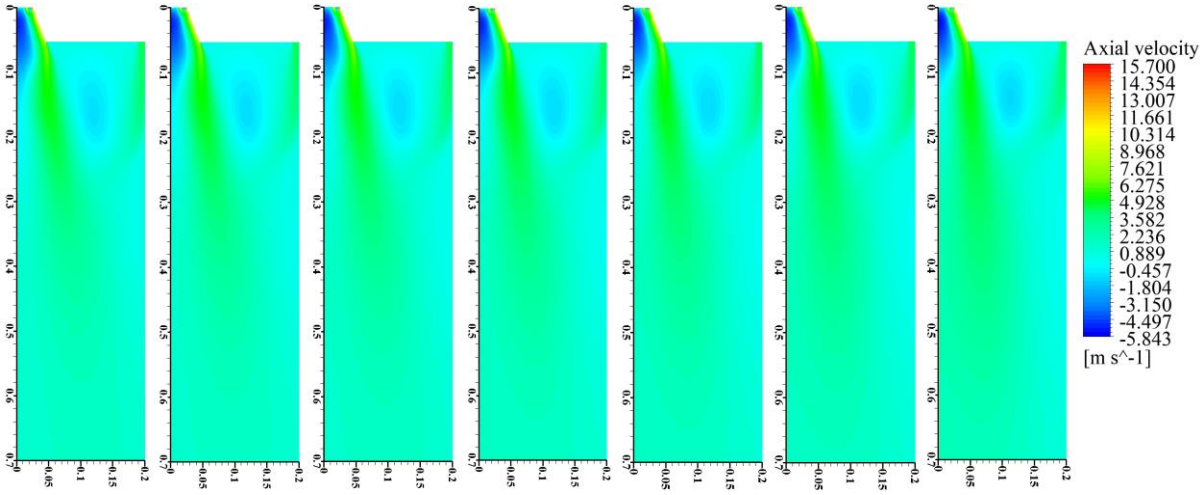

(a) **(b)** **(c)** **(d)** **(e)** **(f)** **(g)**

Fig. 5.1. Contour of axial velocity distribution (m/s) under the studied combustion cases having **(a)** 0% H_2O **(b)** 10% H_2O **(c)** 20% H_2O **(d)** 30% H_2O **(e)** 40% H_2O **(f)** 50% H_2O and **(g)** oxy-steam combustion

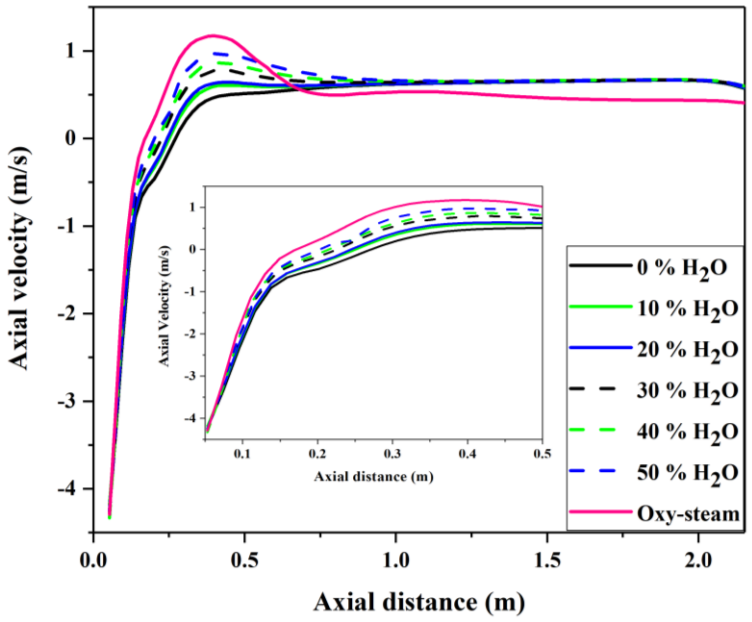

Fig. 5.2. Axial profile of axial velocity (m/s) along centerline for the studied combustion cases

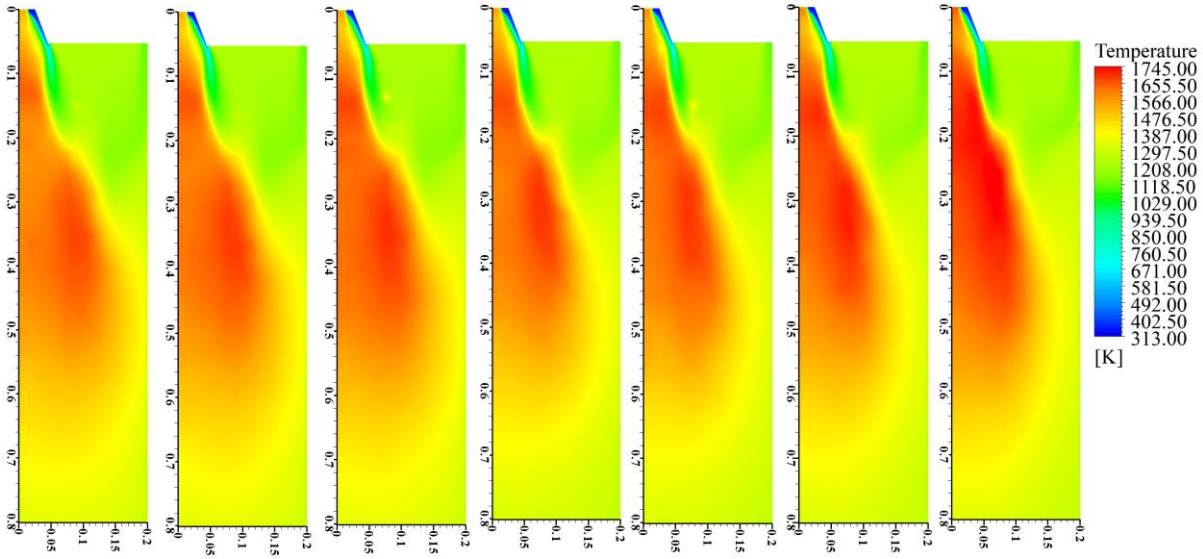

(a) **(b)** **(c)** **(d)** **(e)** **(f)** **(g)**

Fig. 5.3. Contour of temperature distribution under various oxy-fuel combustion cases having **(a)** 0% H_2O **(b)** 10% H_2O **(c)** 20% H_2O **(d)** 30% H_2O **(e)** 40% H_2O **(f)** 50% H_2O and **(g)** oxy-steam combustion

Fig. 5.4 displays the axial profile of temperature distribution under oxy-coal combustion cases (having 0-50% H_2O in the oxidizer) and oxy-steam combustion case (H_2O replaces CO_2 in the oxidizer). With an increase in steam concentration, the position of highest temperature moves downstream. The value of peak temperature also increases with increasing steam content in the oxidizer. Peak temperature obtained under the oxy-steam case is around 10% higher than ideal dry recycle case (0% H_2O) and 2-5% higher than the wet oxy-coal combustion cases having 50-10% H_2O in the oxidizer. With an increase in steam content in oxidizer, the temperature gradient close to the burner region (high-temperature zone) decreases. Char gasification reaction enhances whereas char oxidation reactions attenuate with an increase in the steam concentration of the oxidizer. The temperature distribution inside the combustion chamber is strongly affected by enhanced gasification reactions under steam rich combustion conditions. With increasing steam content, the gasification reactions take place earlier in the region near to the quarl. As gasification reactions are endothermic, the bulk temperature near the quarl reduces, which results in the reduced oxidation rate of volatiles and longer ignition delay in that area. That's why the position of highest temperature moved downstream as the steam concentration in the oxidizer increases.

Fig. 5.5 (a) shows the influence of H_2O addition in the oxidizer on the length of internal recirculation zone formed near the axis of the furnace. The internal recirculation zone (IRZ) slightly shrinks with steam addition in the oxidizer (see Fig. 5.1). Reduction in length of internal recirculation zone (IRZ) is observed with steam addition. Oxy-steam combustion case has the shortest internal recirculation zone (IRZ). The IRZ length is

reduced by 35% in oxy-steam combustion case than the ideal dry recycle oxy-coal combustion case (0% H_2O).

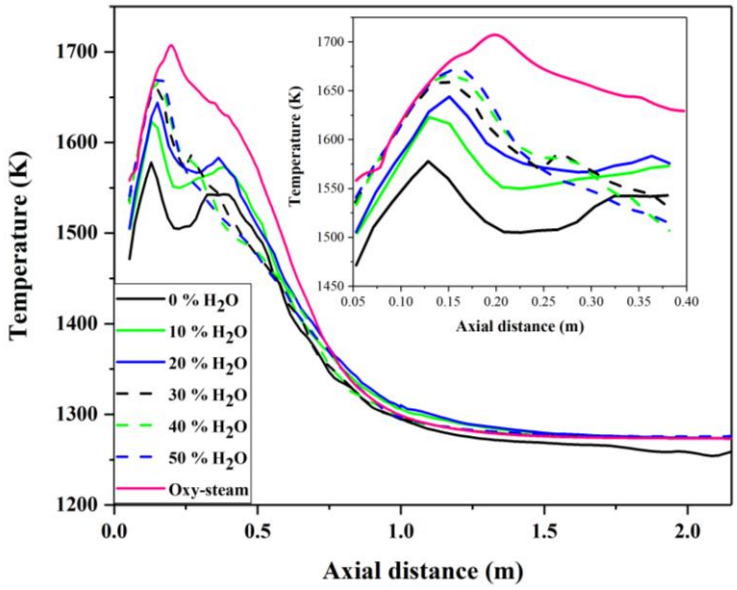

Fig. 5.4. Axial variation of temperature under various oxy-fuel combustion cases having 0-50% H_2O in oxidizer and oxy-steam combustion case

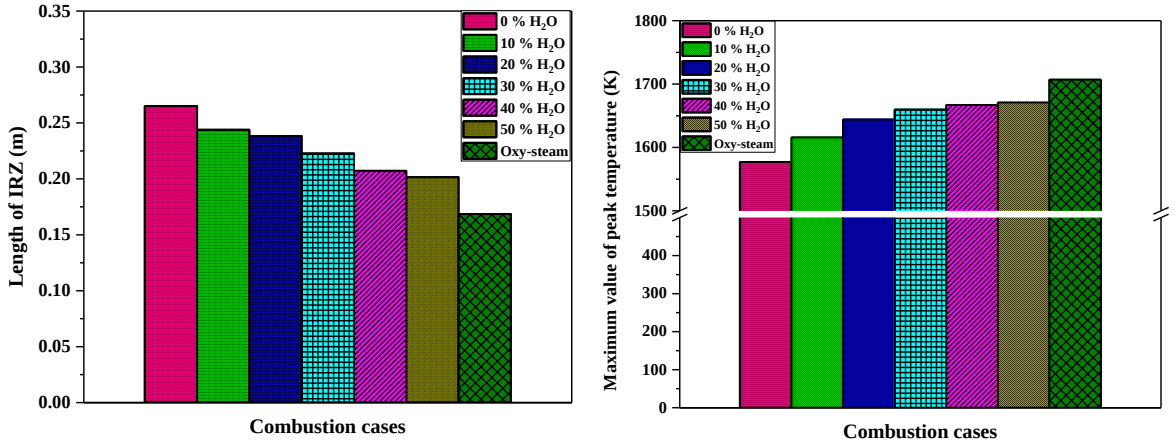

(a) **(b)**

Fig. 5.5. Influence of various combustion environment obtained by varying steam content of oxidizer on **(a)** length of internal recirculation zone (IRZ) and **(b)** maximum temperature (K)

Fig. 5.5 (b) displays the influence of H_2O addition in the oxidizer on the maximum temperature obtained along the centerline of the furnace. The peak temperature obtained under the oxy-steam case is around 10% higher than ideal dry recycle case (0% H_2O) and 2-5% higher than the wet oxy-coal combustion cases having 50-10% H_2O in the oxidizer.

5.2.2 Oxidizer Distribution and Radiative Heat Transfer

Fig. 5.6 shows the contour of oxygen mole fraction under oxy-coal combustion cases (having 0-50% H_2O in the oxidizer) and oxy-steam combustion case (H_2O replaces CO_2 in the oxidizer). Char gasification reactions are enhanced with an increase in H_2O concentration in the oxidizer due to faster oxygen diffusion rate under enriched steam combustion atmosphere. Enhanced gasification reactions resulted in increase in oxygen consumption close to the burner quarl under the combustion cases having higher H_2O concentration. The oxygen mole fraction distribution profile has considerable influence only close to the burner quarl, where oxygen consumption is increased due to enhanced gasification reactions at higher steam concentration.

Axial variation of incident radiation under oxy-coal combustion cases (having 0-50% H_2O in the oxidizer) and oxy-steam combustion case (H_2O replaces CO_2 in the oxidizer) is shown in Fig. 5.7. The accurate profile of incident radiation inside the combustion chamber has a dependency on temperature distribution as radiative heat transfer is computed as the fourth power of the temperature. As we discussed earlier, the increase in H_2O concentration in the oxidizer would increase the flame temperature due to the reduced gaseous volume

heat capacity. The peak of incident radiation shifted towards the downstream of the furnace with an increase in H_2O concentration in the oxidizer.

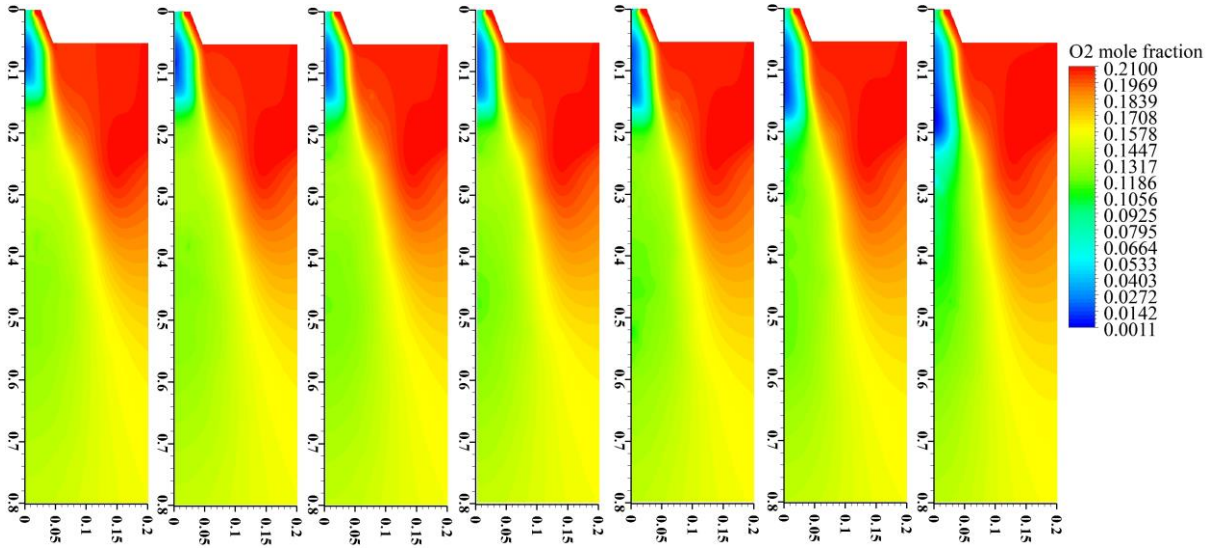

(a) **(b)** **(c)** **(d)** **(e)** **(f)** **(g)**

Fig. 5.6 Contour of oxygen mole fraction distribution under various oxy-coal combustion cases having **(a)** 0% H_2O **(b)** 10% H_2O **(c)** 20% H_2O **(d)** 30% H_2O **(e)** 40% H_2O **(f)** 50% H_2O **(g)** oxy-steam

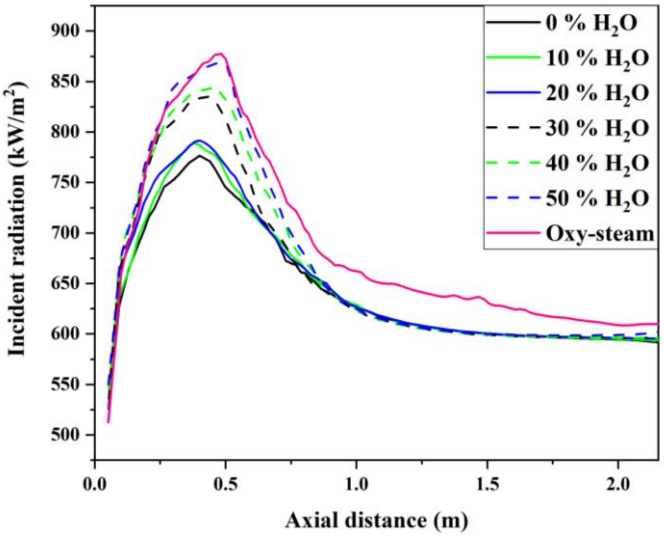

Fig. 5.7 Axial variation of incident radiation under various oxy-fuel combustion cases having 0-50% H_2O in oxidizer and oxy-steam combustion case

5.2.3 Temporal History of Particle

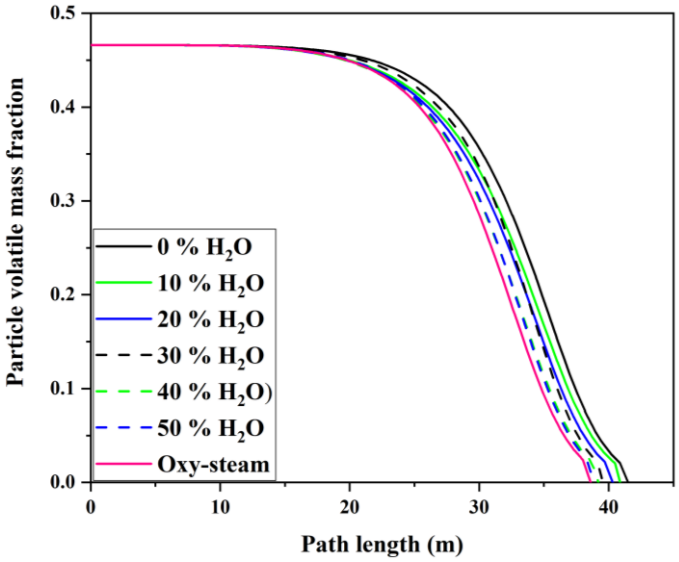

Fig. 5.8 Temporal variation of particle volatile mass fraction under various oxy-fuel combustion cases having 0-50% H_2O in oxidizer and oxy-steam combustion case (d=95.9 µm)

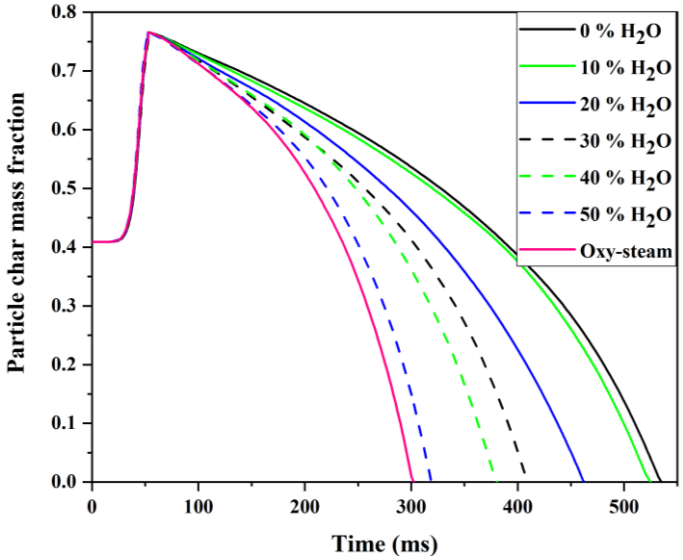

Fig. 5.9 Temporal variation of particle char mass fraction under various oxy-fuel combustion cases having 0-50% H_2O in oxidizer and oxy-steam combustion case (d=95.9 µm)

The temporal profile of particle volatile and particle char mass fraction of 95.9 µm particle under oxy-coal combustion cases (having 0-50% H_2O in the oxidizer) and oxy-steam combustion case (H_2O replaces CO_2 in the oxidizer) is displayed in Fig. 5.8 and Fig. 5.9. There are four stages of pulverized coal combustion: drying, devolatilization, volatile combustion and char combustion. The volatiles are released into gas phase during the devolatilization process. After the completion of the devolatilization process, char combustion initiates. Char is consumed by both oxidation and gasification reactions; thus, the char mass fraction diminishes and finally reduces to zero at the burnout. The time required for the completion of devolatilization decreases with an increase in H_2O concentration in the oxidizer. The influence of H_2O addition in the oxidizer is dominant on particle char mass fraction than the particle volatile mass fraction. With an increase in H_2O concentration in the oxidizer, gasification reaction enhances at the coal particle surface and work favorably in the burnout. Enhanced burnout is obtained at higher steam concentration, that is a significant reason behind faster depletion of char mass fraction of the particle.

5.2.4 Distribution of Species

The axial variation of O_2, CO_2 and H_2O mole fraction under oxy-coal combustion cases (having 0-50% H_2O in the oxidizer) and oxy-steam combustion case (H_2O replaces CO_2 in the oxidizer) is displayed in Fig. 5.10-5.12. The oxygen-deficient zone adjacent to the burner created due to intense oxidation of volatiles can be observed in the axial profile of O_2 mole fraction distribution in Fig. 5.10. With an increase in H_2O concentration in the oxidizer, oxygen deficient zone slightly extended. The largest oxygen deficient area has

been obtained for oxy-steam combustion case. With an increase in H_2O concentration in the oxidizer, the gaseous volume heat capacity decreases and the rate of O_2 diffusion increases (Yu et al., 2013). Oxygen consumption has been increased under enriched steam combustion cases close to the burner. The oxy-coal combustion cases having 0-50% H_2O concentration in the oxidizer has almost similar shape of O_2 mole fraction along the centerline of the combustion chamber.

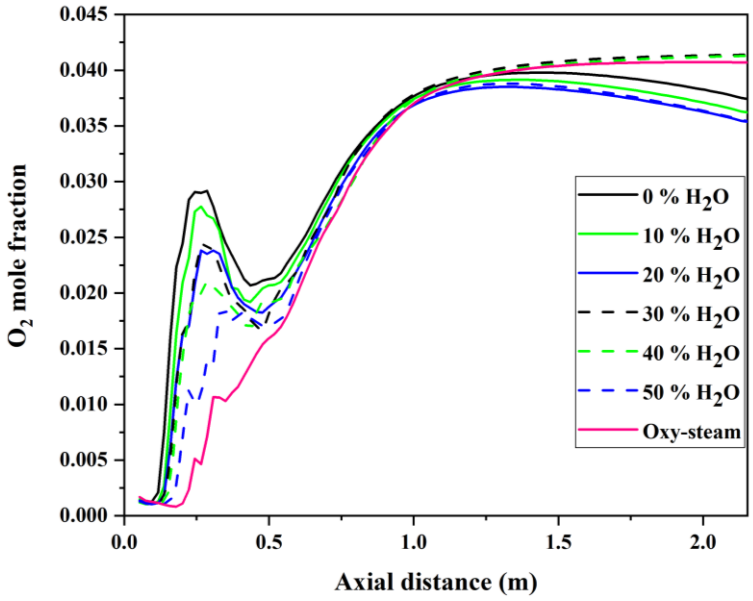

Fig. 5.10 Axial variation of O_2 mole fraction under various oxy-fuel combustion cases having 0-50% H_2O in oxidizer and oxy-steam combustion case

During the addition of H_2O in the oxidizer, an equal amount of CO_2 has been replaced by H_2O, which results in a decrease in CO_2 mole fraction (see Fig. 5.11). The peak of CO_2 mole fraction has been obtained at the axial position of 0.625 m from the burner exit. After axial location 0.625 m, the axial profile of CO_2 mole fraction is almost constant or decays at a prolonged rate. The gradient of CO_2 mole fraction reduces with an increase in H_2O concentration in the oxidizer. Highest and lowest gradient of CO_2 mole fraction has been

obtained for dry recycle oxy-coal combustion case and oxy-steam combustion case, respectively.

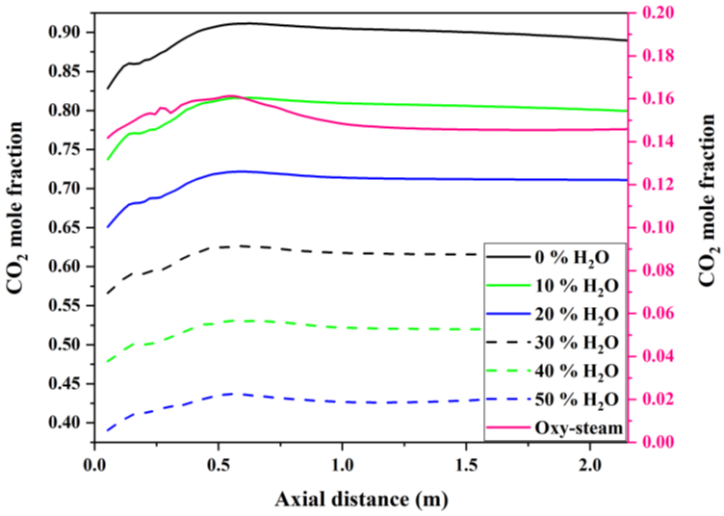

Fig. 5.11 Axial variation of CO_2 mole fraction under various oxy-fuel combustion cases having 0-50% H_2O in oxidizer and oxy-steam combustion case

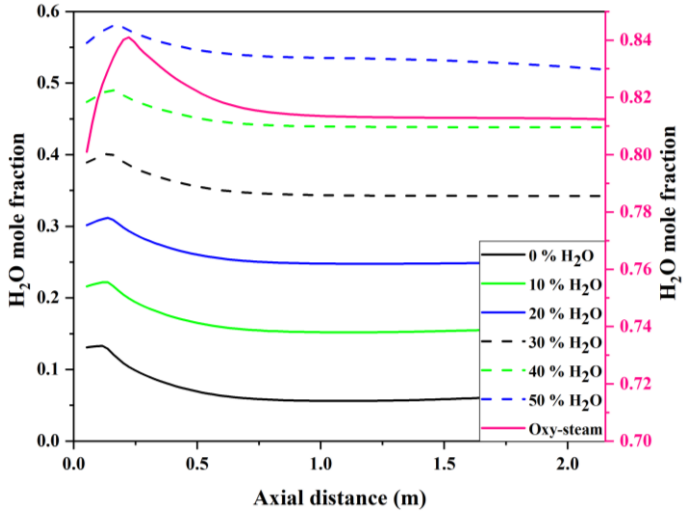

Fig. 5.12 Axial variation of H_2O mole fraction under various oxy-fuel combustion cases having 0-50% H_2O in oxidizer and oxy-steam combustion case

The mole fraction of H_2O rises with an increase in H_2O content in the oxidizer due to the replacement of an equal amount of CO_2 with the H_2O in the oxidizer. Oxy-coal combustion case having 0% H_2O in the oxidizer has produced peak H_2O mole fraction at axial location

~0.11 m from the burner exit. With an increase in H_2O content in the oxidizer, the peak shifts along the axial direction. Oxy-steam combustion case has peak H_2O mole fraction at axial location ~0.22 m from the burner exit. The presence of higher H_2O concentration enhances the endothermic steam char gasification reaction producing CO and H_2. CO and H_2 produced by gasification reaction are beneficial to the ignition and combustion of the homogeneous gaseous mixture.

The axial variation of CO mole fraction under oxy-coal combustion cases (having 0-50% H_2O in the oxidizer) and oxy-steam combustion case (H_2O replaces CO_2 in the oxidizer) is shown in Fig. 5.13. Both char oxidation (Eq^n 3.39) and char gasification (Eq^n 3.40) reactions produces CO. The CO mole fraction distribution profile is important only for the region near the burner exit. After axial location greater than 0.6 m, CO mole fraction has been negligible for all the combustion cases considered. CO mole fraction increases with an increase in steam concentration in the oxidizer due to enhanced gasification reaction in the presence of H_2O.

The axial variation of H_2 mole fraction under oxy-coal combustion cases (having 0-50% H_2O in the oxidizer) and oxy-steam combustion case (H_2O replaces CO_2 in the oxidizer) is shown in Fig. 5.14. As it can be seen from Eq^n (3.41), H_2 is produced by steam-char gasification reaction. The steam char gasification reaction takes place immediately after volatile release due to low heat consumption and smaller activation energy. It can be seen from Fig. 5.14 that the mole fraction of H_2 is proportional to the amount of steam added in the oxidizer. The position of peak H_2 mole fraction also shifts towards the axial direction with an increase in H_2O mole fraction in oxidizer. Faster ignition under enriched steam

combustion condition is consistent with the experimental findings of Zou et al. (2015), which states that sooner ignition occur in O_2/H_2O combustion condition.

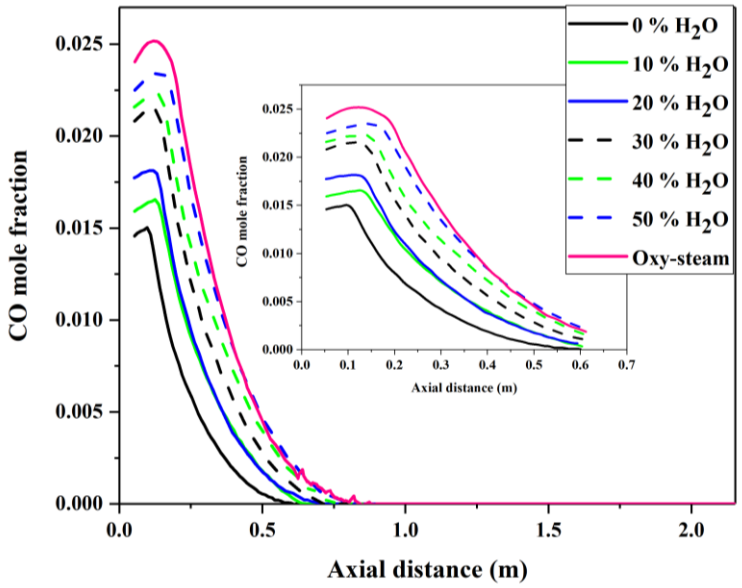

Fig. 5.13 Axial profile of CO mole fraction under various oxy-fuel combustion cases having 0-50% H_2O in oxidizer and oxy-steam combustion case

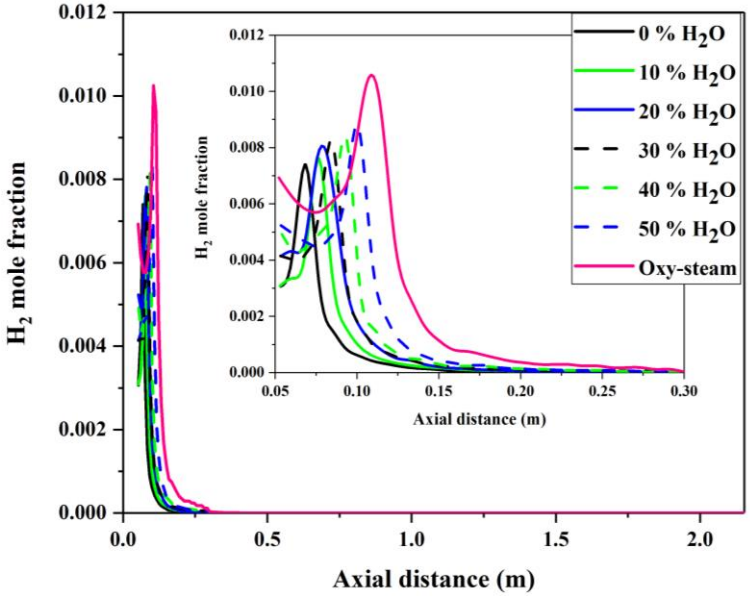

Fig. 5.14 Axial profile of H_2 mole fraction under various oxy-fuel combustion cases having 0-50% H_2O in oxidizer and oxy-steam combustion case

5.3 Influence of Gasification Reactions

After the completion of the devolatilization process, combustion of char initiates. The char combustion can be described by heterogeneous reactions (Eq^n 3.39-3.41) at the char particle surface. The heterogeneous reactions represent the oxidation (Eq^n 3.39) and gasification (Eq^n 3.40-3.41) reactions at the char particle surface. This section investigates the effect of the gasification reactions (Eq^n 3.40-3.41) on species concentration and temperature profile under oxy-fuel combustion atmosphere. Here w/o GR and with GR combustion case represent oxy-coal combustion case without and with consideration of gasification reactions.

Fig. 5.15 shows the axial profile of temperature distribution for both with and without consideration of gasification reactions. Difference between temperature profile is attributed due to the endothermic nature of gasification reactions. The influence of the gasification reactions is noticeable from the entrance of the combustion chamber to an axial location 1.0 m. In this zone, the negative value of ΔT (where ΔT is temperature difference of with GR and without GR combustion case) can be observed due to the endothermic nature of the gasification reaction. A remarkable reduction (~80 K) in predicted temperature is obtained due to endothermic gasification reactions at the char particle surface.

From the profiles of CO_2 and H_2O mass fraction, the amount of CO_2 and H_2O consumed in gasification reaction can be observed in Fig. 5.16. The gap between w/o GR curve and with GR curve represents the consumed amount of CO_2 and H_2O. The gap between w/o GR and with GR curve is found at an axial location less than ~1.0 m. In this zone, CO_2 and H_2O molecules react with coal char, and endothermic gasification reactions takes place.

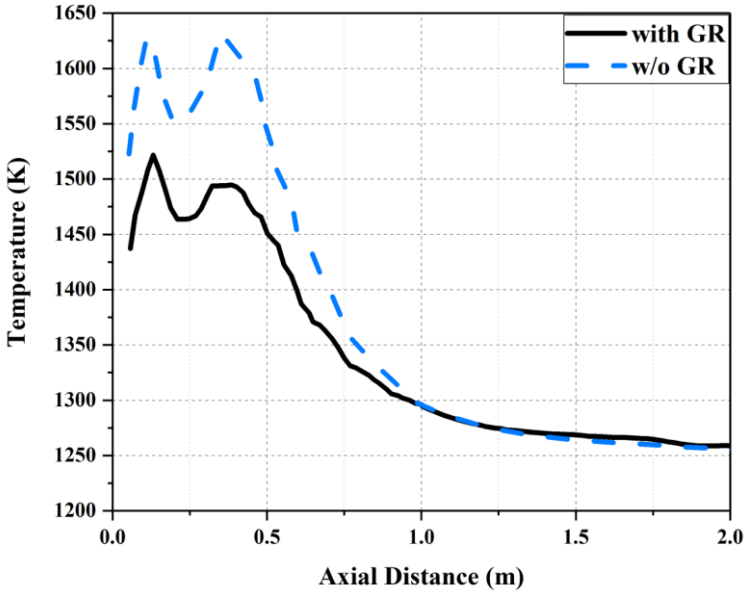

Fig. 5.15. Axial variation of predicted temperature with and without consideration of gasification reaction

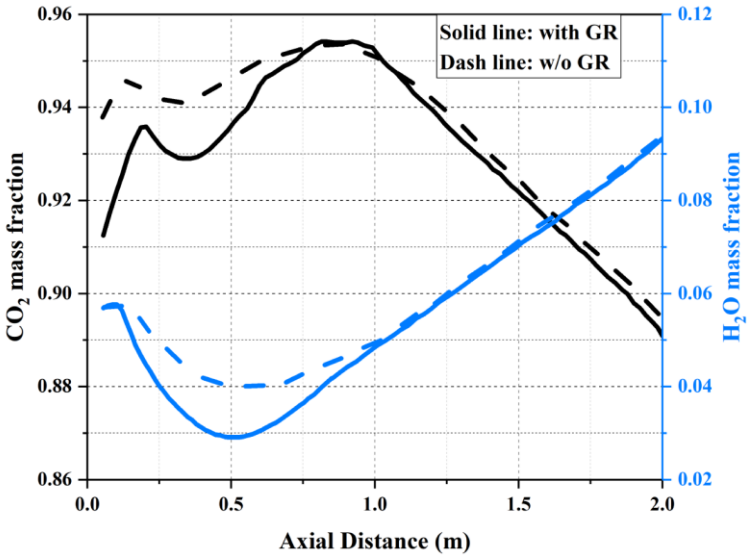

Fig. 5.16. Axial variation of predicted CO_2 and H_2O mass fraction with and without consideration of gasification reaction

The zone (extending approximately up to 1.0 m axial location) having the influence of gasification reactions on CO_2 and H_2O mass fraction is consistent with its influence on the

temperature profile. This zone is termed as gasification zone, and the influence of the gasification reactions exists only within this zone.

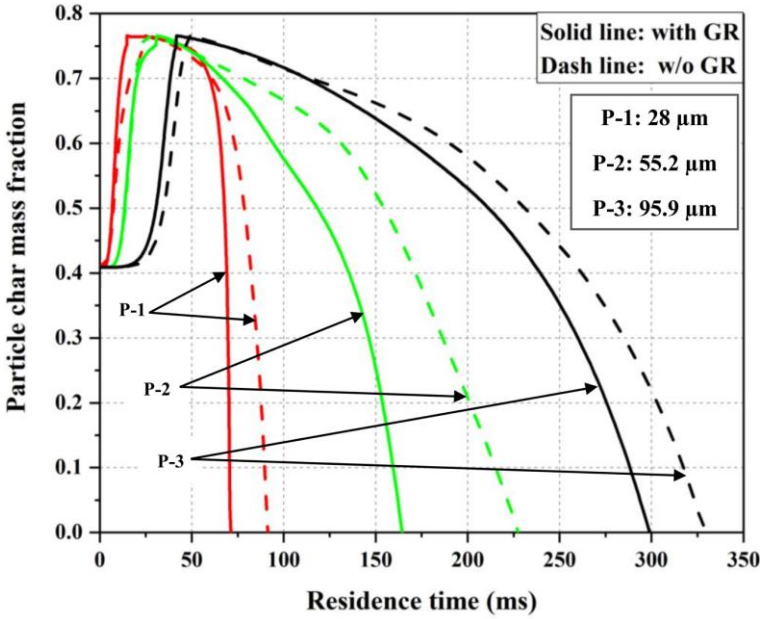

Fig. 5.17. Profiles of particle char mass fraction v/s residence time

Particle char mass fraction profile for three particle sizes of 28 µm, 55.2 µm and 95.9 µm, for both with and without consideration of gasification reactions, is shown in Fig. 5.17. Char mass fraction profile has three stages: particle heating, volatile release and char burnout (Mao et al., 2016). In the heating stage, the char mass fraction remains constant. In the second stage, the increase in temperature releases moisture and volatile matter; hence, particle char mass fraction rises, as shown in Fig. 5.17. In the third stage, combustion of char particle initiates, and char is consumed by O_2, CO_2 and H_2O resulting in reduced char mass fraction. The consideration of gasification reaction on char particle surface reduces the char burnout time. The gasification reactions enhance char consumption, and the results are in accordance with the findings of Zhou et al. (2017). The char-CO_2 gasification

reaction creates additional porosity on the char surface. Hence, char burnout improves with the consideration of gasification reactions under O_2/CO_2 combustion atmosphere (Hecht et al., 2012).

5.4 NO_x Emission Characteristics of Oxy-Coal Combustion

In this section, NO_x emission characteristics of oxy-coal combustion have been thoroughly investigated employing the developed and validated numerical model under oxy-coal combustion atmosphere. The NO_x emission (ppm) produced under the various oxy-coal combustion atmosphere obtained by varying the composition of oxidizer, under various inlet temperature and pressure of feed gas has been studied. Influence of higher concentration steam addition on NO_x emission under oxy-coal combustion atmosphere has also been assessed employing the developed oxy-coal combustion model. Furthermore, a quantitative summary of NO_x emission at the outlet of the combustion chamber under above-mentioned operating conditions have been provided.

5.4.1 Validation

Fig. 5.18 compares the radial profile of NO_x concentration (ppm) predicted by current numerical simulation with the Experimental result of Toporov et al. (2008) and numerical result of Gaikwad et al. (2017) at four axial locations from the burner exit (X=0.05 m, X=0.2 m, X=0.3 m and X=0.5 m). The nitrogen content in coal is the major contributor in NO_x formation through the fuel NO_x formation mechanism. At axial location 0.05 m from the burner exit significant deviation between current numerical result and experimental data

has been found. The temperature profile (shown in Fig. 3.7) also has significant deviation from experimental data at axial locations close to the burner exit due to model's inability to predict a strong recirculation zone created by the penetration of burner cold stream.

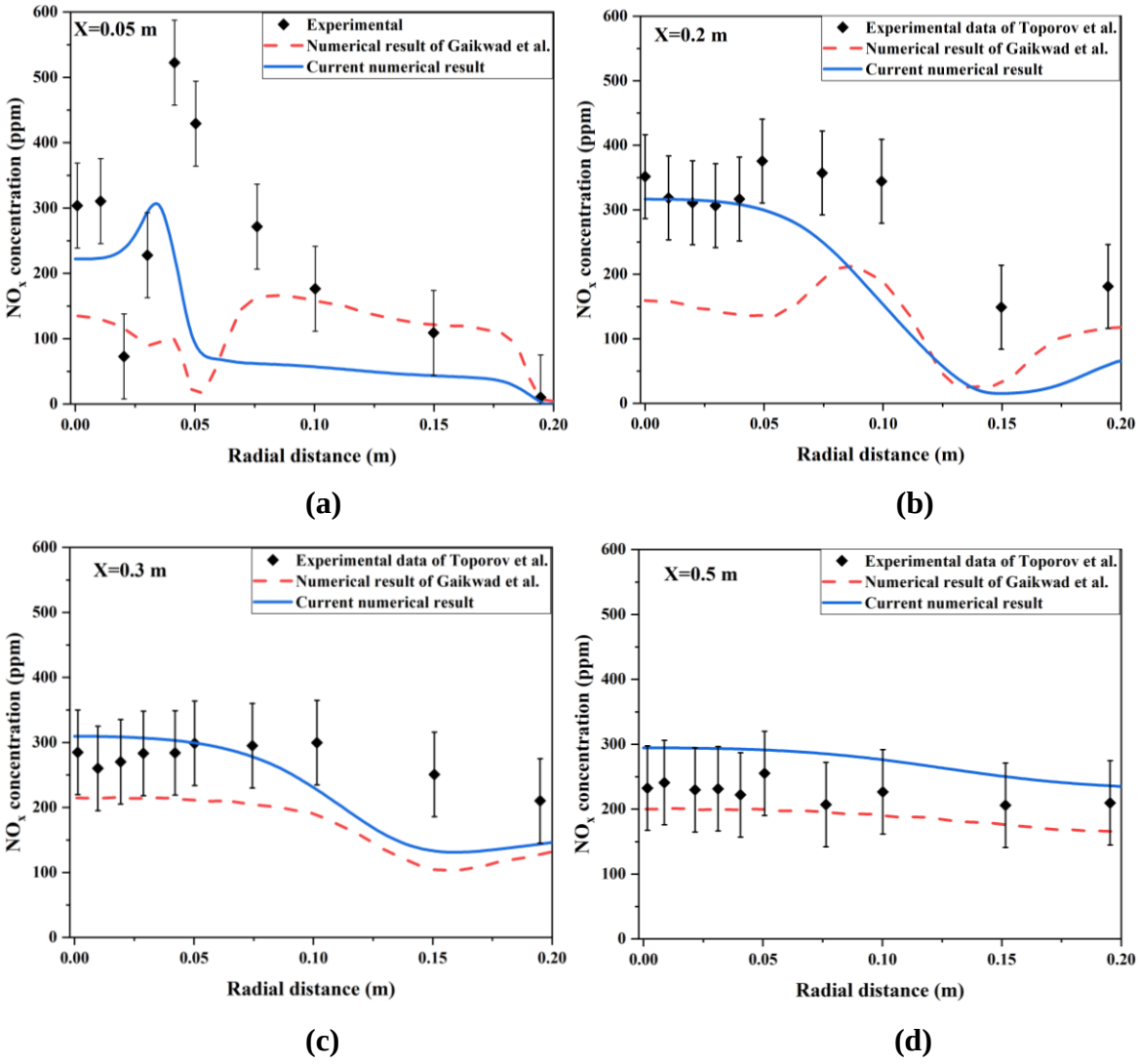

Fig. 5.18. Comparison of current numerical result of NO_x concentration (ppm) with experimental data and available numerical result at different axial locations from burner **(a)** 0.05 m **(b)** 0.2 m **(c)** 0.3 m and **(d)** 0.5 m

At axial location 0.2 m from the burner exit, numerical modelling results have good agreement with the experimental data at inner radial positions (0<R<0.05 m), whereas

towards the outer radial locations the deviation between numerical modelling results and experimental data is in the range of 15-20%. At axial locations 0.3 m and 0.5 m from the burner exit, numerical modelling results are in good agreement with the experimental data of NO_x concentration. The current simulation results are also compared with the numerical results of Gaikwad et al. (2017) on the same combustion test facility. As it can be seen in Fig. 5.18, overall an acceptable agreement has been found between the numerical simulation results and experimental data. Although there are some discrepancies in the numerical simulation result and experimental data at certain location. The current numerical simulation results are able to capture qualitative trend of NO_x concentration profile.

5.4.2 Influence of Combustion Environment on NO_x Emission

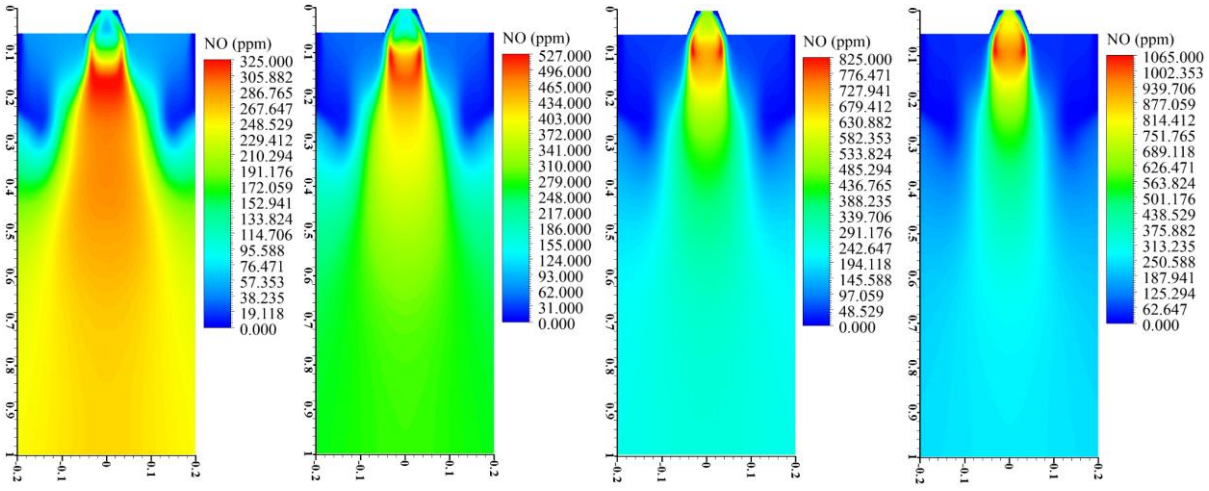

(a) **(b)** **(c)** **(d)**

Fig. 5.19. Distribution of NO_x concentration (ppm) inside the combustion chamber under various oxy-coal combustion cases **(a)** 21% O_2/79% CO_2 **(b)** 25% O_2/75% CO_2 **(c)** 30% O_2/70% CO_2 **(d)** 35% O_2/65% CO_2

Fig. 5.19 shows the contour of NO_x concentration (ppm) under various oxy-coal combustion atmospheres obtained by changing composition of oxidizer. Increase in NO_x concentration (ppm) has been observed with an increase in O_2 concentration. Oxy-fuel combustion cases having O_2 concentration 25%, 30% and 35% have 60%, 150% and 225% higher NO_x concentration (ppm) than the 21% O_2 oxy-coal combustion case. With an increase in oxygen concentration conversion rate of coal N to NO_x has been enhanced (Al-Abbas et al., 2013), which ultimately results in higher NO_x concentration inside the combustion chamber.

Fig. 5.20 displays the influence of the various oxy-coal combustion atmosphere on the radial profile of NO_x concentration (ppm) at axial locations 0.05 m, 0.2 m 0.3 m and 0.5 m from burner exit. Rise in oxygen level in the oxidizer increases the NO_x concentration at all four axial locations. At axial location 0.05 m from burner exit, maximum peak of NO_x concentration increases by an increase in oxygen level in the oxidizer. All four oxygen levels have identical NO_x concentration profile towards the outer radial location. At axial location 0.2 m and 0.3 m from burner exit, earlier decay in NO_x concentration profile can be observed for higher oxygen level (35% and 30% O_2) compared to lower oxygen levels (21% and 25% O_2). At axial location 0.5 m from the burner exit, the variation of NO_x concentration is minimum among all axial locations. At this axial location, slightly higher gradient of NO_x concentration is observed towards inner radial location ($0<R<0.1$ m) than the outer radial location ($0.1<R<0.2$ m) under all four oxy-coal combustion cases.

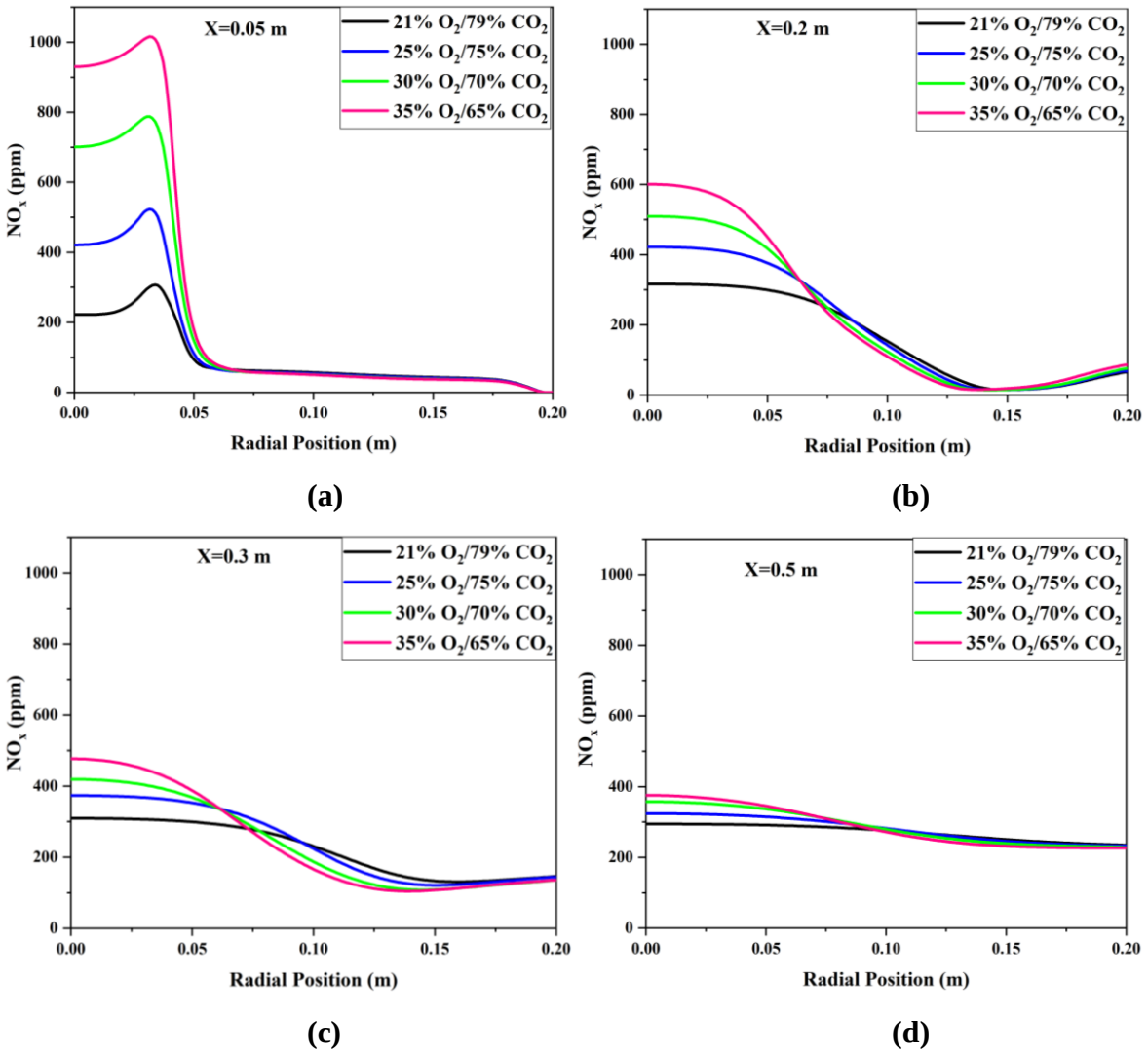

Fig. 5.20. Influence of various oxy-coal combustion atmosphere on radial profile of NO_x concentration (ppm) at different axial locations **(a)** 0.05 m **(b)** 0.2 m **(c)** 0.3 m and **(d)** 0.5 m

5.4.3 Influence of Inlet Temperature and Pressure of Feed Gas on NO_x Emission

Influence of inlet temperature of feed gas on NO_x concentration (ppm) distribution inside the combustion chamber is shown in Fig. 5.21. The NO_x concentration contour is shown up to axial location of 1.0 m inside the combustion chamber as NO_x concentration does not

have significant variation towards the downstream of the combustion chamber. At higher inlet feed gas temperature (500 K and 800 K), initiation of NO_x formation starts earlier than the inlet feed gas temperature of 313 K. With an increase in inlet feed gas temperature the volatiles present in coal particles are evolved earlier and char combustion initiates within the quarl of burner. Due to faster volatile release in gas phase and earlier initiation of char combustion, the flame front shifted near to the burner. The shifting of flame front region towards the burner is responsible for earlier initiation of NO_x formation at higher inlet feed gas temperature. At higher inlet feed gas temperature, the conversion of vol_N and char_N into NO_x is also enhanced, which resulted into increases in NO_x concentration (ppm) with an increase in inlet feed gas temperature. Increasing inlet feed gas temperature from 313 K to 500 K and 800 K, increases maximum NO_x concentration (ppm) inside the combustion chamber by 67% and 123% respectively.

Fig. 5.22 displays the effect of the inlet feed gas temperature on radial profile of NO_x concentration (ppm) at axial locations 0.05 m and 0.2 m from burner exit. At axial location 0.05 m, increasing inlet feed gas temperature from 313 K to 500 K, the peak of NO_x concentration (ppm) obtained is almost doubled. Increase in inlet feed gas temperature from 500 K to 800 K, the radial profile has only slight variations. Towards the outer radial locations (R>0.1 m), higher inlet feed gas temperatures (500 K and 800 K) have lower NO_x concentration. At higher inlet feed gas temperatures narrower flames have been obtained, which is the major reason behind lower NO_x concentration towards outer radial position. At axial location 0.2 m from burner exit, NO_x concentration is slightly higher for 500 K and 800 K feed gas temperature in inner radial position (0-0.075 m). Towards outer radial

position the minima value of NO_x concentration decreases with increasing inlet feed gas temperature.

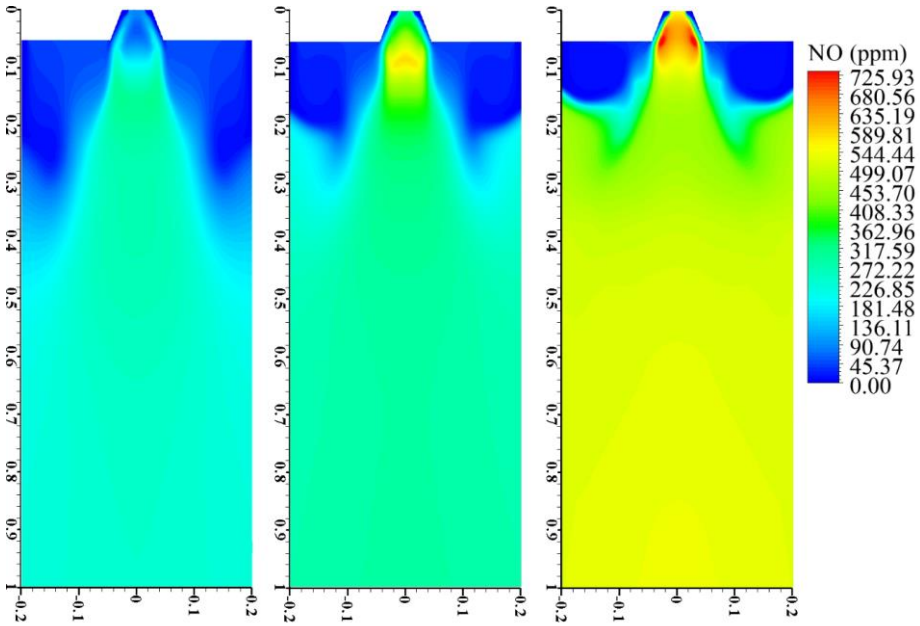

(a) **(b)** **(c)**

Fig. 5.21. Distribution of NO_x concentration (ppm) inside the combustion chamber under various inlet feed gas temperature **(a)** 313 K **(b)** 500 K **(c)** 800 K

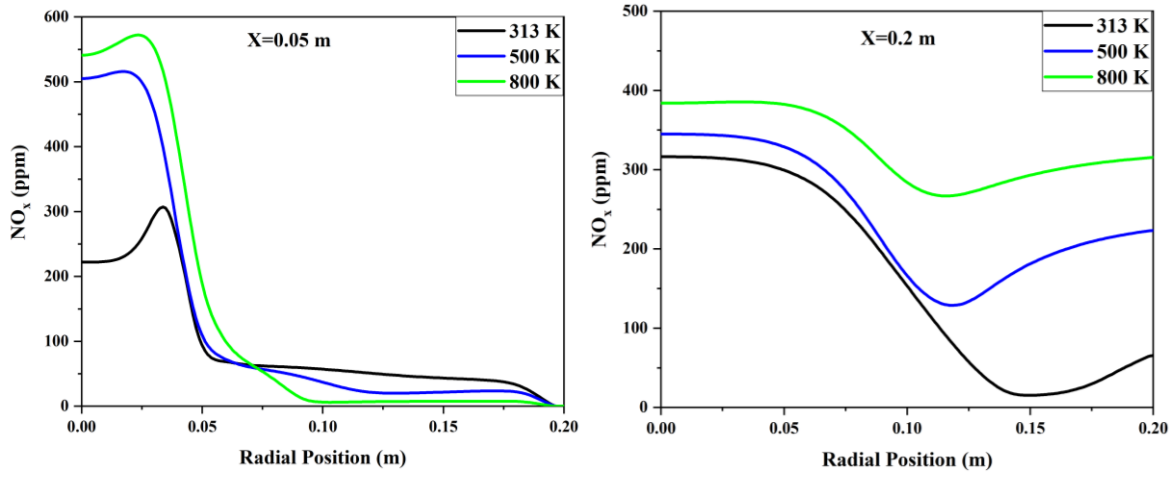

(a) **(b)**

Fig. 5.22. Effect of the inlet feed gas temperature on radial profile of NO_x concentration (ppm) at axial locations **(a)** 0.05 m and **(b)** 0.2 m

Influence of inlet pressure of feed gas on NO_x concentration (ppm) distribution inside the combustion chamber is shown in Fig. 5.23. At higher inlet feed gas pressures (5 bar and 10 bar), initiation of NO_x formation starts earlier than the inlet feed gas pressure of 1 bar. With an increase in inlet feed gas pressure the flame propagation speed slower down due to higher density of gaseous phase at higher pressure. Lower flame propagation speed results into initiation of earlier combustion of coal particles, which ultimately results in shorter and narrower flames. The maximum NO_x concentration (ppm) inside the combustion chamber for inlet feed gas pressure of 5 bar and 10 bar, increases by 13% and 41% than the inlet feed gas pressure of 1 bar.

Fig. 5.24 displays the effect of the inlet feed gas pressure on radial profile of NO_x concentration (ppm) at axial locations 0.05 m and 0.2 m from burner exit. At axial location 0.05 m, the peak NO_x concentration (ppm) increased by 6% and 23% with an increase in inlet feed gas pressure from 1 bar to 5 bar and 10 bar, respectively. At this axial location, inner radial position has higher NO_x concentration (ppm), whereas outer radial position has lower NO_x concentration (ppm) at higher inlet feed gas pressures (5 bar and 10 bar). Short and narrow flame front obtained at higher inlet feed gas pressures (5 bar and 10 bar) is the major reason for this kind of radial profile. At axial location 0.2 m from burner exit, gradient of NO_x concentration (ppm) is highest for 1 bar inlet feed gas pressure and lowest for 10 bar inlet feed gas pressure. Comparatively lower value of NO_x concentration has been observed for inlet feed gas pressures (5 bar and 10 bar) than the 1 bar.

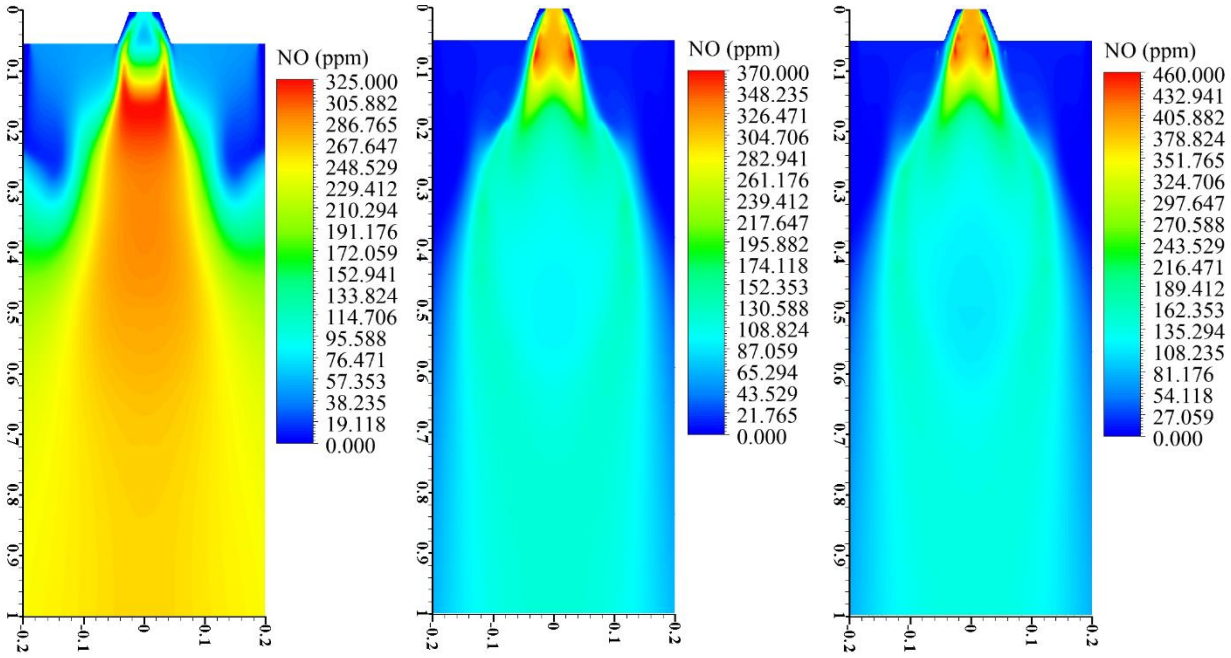

(a) **(b)** **(c)**

Fig. 5.23. Distribution of NO_x concentration (ppm) inside the combustion chamber under various inlet feed gas pressure **(a)** 1 bar **(b)** 5 bar and **(c)** 10 bar

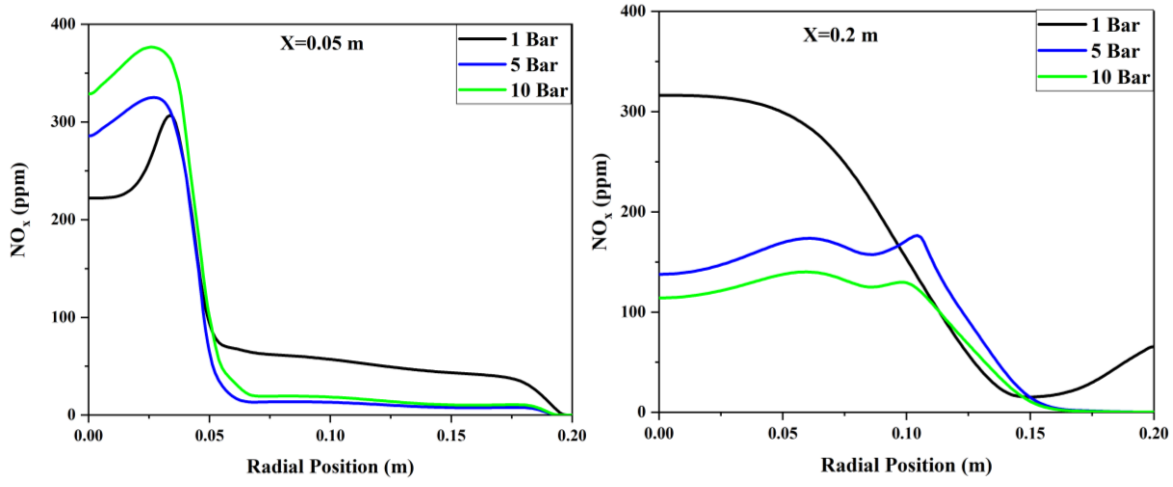

(a) **(b)**

Fig. 5.24. Effect of the inlet feed gas pressure on radial profile of NO_x concentration (ppm) at axial locations **(a)** 0.05 m and **(b)** 0.2 m

5.4.4 Influence of Steam Addition on NO_x Emission

The contour of NO_x concentration (ppm) under ideal dry-recycle oxy-coal combustion (0% H_2O), two wet recycle oxy-coal combustion cases (20% and 40% H_2O in the oxidizer) and oxy-steam combustion case (whole CO_2 is replaced by H_2O in the oxidizer) is sown in Fig. 5.25. With an increase in H_2O concentration in the oxidizer, the maximum NO_x concentration (ppm) inside the combustion chamber has increased significantly. The char_N conversion to NO has been enhanced under enriched steam combustion atmosphere, which ultimately resulted in increased NO_x concentration inside the combustion chamber. The result of increased NO_x concentration with an increase in H_2O concentration in the oxidizer is consistent with the findings of Tu et al. (2015b). From the contour of NO_x concentration, it can be seen that the maximum NO_x concentration (ppm) obtained inside the combustion chamber under oxy-fuel combustion cases having 20% and 40% H_2O in the oxidizer (wet recycle combustion case) is 1.7 times and 2.35 times higher than the maximum NO_x concentration of oxy-fuel combustion case having 0% H_2O (ideal dry-recycle combustion case). The maximum NO_x concentration (ppm) of oxy-steam combustion case is 3.0 times higher than the oxy-fuel combustion case having 0% H_2O.

Fig. 5.26 displays the radial profile of NO_x concentration (ppm) at axial locations 0.05 m and 0.2 m from burner exit for oxy-coal combustion cases having steam content from 0-50% in oxidizer and oxy-steam combustion case. Increasing H_2O concentration level in oxidizer increases the NO_x concentration at both the axial locations. At axial location 0.05 m from burner exit, the peak of NO_x concentration (ppm) increases by 9%-141% for wet

oxy-coal combustion cases having H_2O concentration (10-50%) in the oxidizer compared to ideal dry recycle oxy-coal case (0% H_2O).

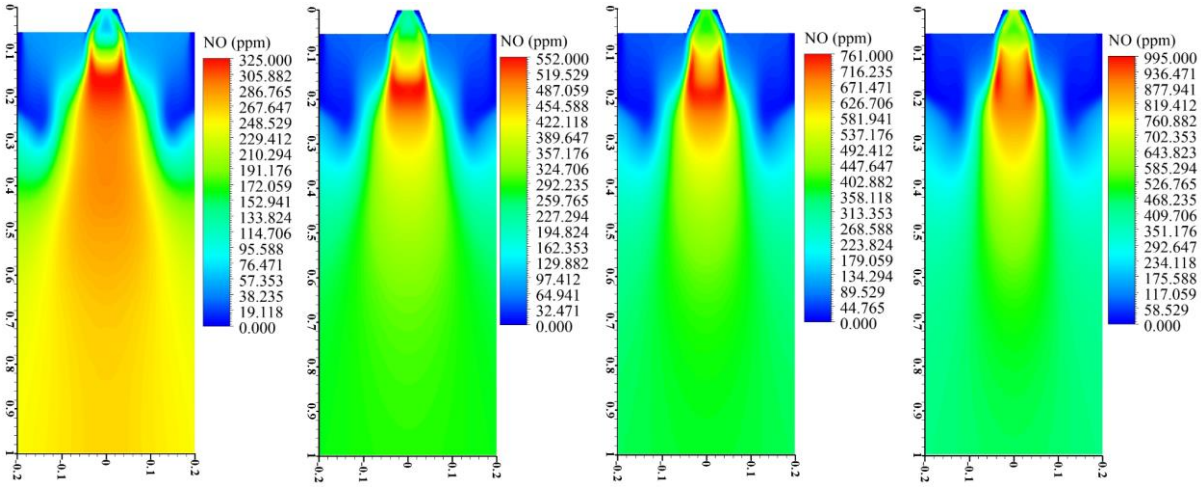

(a) **(b)** **(c)** **(d)**

Fig. 5.25. Distribution of NO_x concentration (ppm) inside the combustion chamber under various wet oxy-coal combustion cases having **(a)** 0% H_2O **(b)** 20% H_2O **(c)** 40% H_2O and **(d)** oxy-steam combustion case

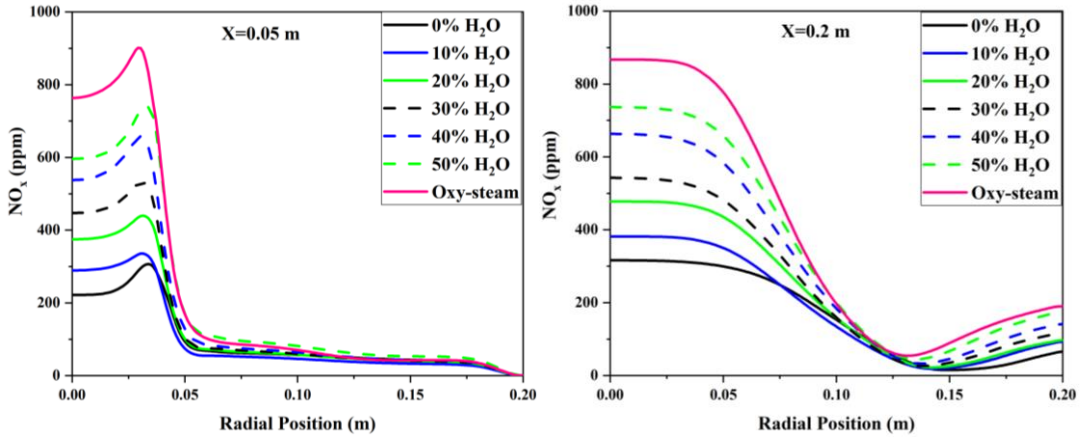

(a) **(b)**

Fig. 5.26. Radial variation of NO_x concentration (ppm) under various oxy-coal combustion cases having 0-50% H_2O in oxidizer and oxy-steam combustion case at axial locations **(a)** 0.05 m and **(b)** 0.2 m

The peak of NO_x concentration (ppm) rises by 193% under oxy-steam combustion case (H_2O replaces whole CO_2 in the oxidizer) compared to ideal dry recycle oxy-coal case (0%

H_2O). At axial location 0.2 m, earlier decay in NO_x concentration profile can be observed for higher H_2O concentration (30%-50% H_2O and oxy-steam combustion case) compared to lower H_2O concentration (0-20% H_2O). The main elementary reaction which attributed an increase in NO_x production under enriched steam combustion atmosphere is $NH+H_2O \Leftrightarrow HNO+H_2$. Thus, the reaction pathway $NH_2 \rightarrow NH \rightarrow HNO \rightarrow NO$ has been predominant under enriched steam combustion atmosphere (Zou et al., 2015).

5.4.5 Quantitative Summary of NO_x Emission (ppm) under Various Operating Conditions

The influence of above discussed parameters on quantitative amount of NO_x concentration at the outlet of combustion chamber is provided in Fig. 5.27. Oxy-coal combustion case having 25%, 30% and 35% O_2 in the oxidizer have 13%, 42% and 68% higher NO_x at the outlet of the combustion chamber (see Fig. 5.27a). From Fig. 5.27 (b), in can be seen that inlet feed gas temperatures of 500 K and 800 K have produced 19% and 45% more NO_x emission (ppm) at the outlet of combustion chamber than the inlet feed gas temperature of 313 K. Although slight increase in NO_x concentration is observed with an increase in inlet feed gas pressure in Fig. 5.23 and Fig. 5.24, but NO_x concentration (ppm) at the outlet of combustion chamber is significantly reduced at higher feed gas pressure. Lower flame propagation speed due to increased density of gaseous phase is the reason behind lower NO_x concentration (ppm) at the outlet of combustion chamber (see Fig. 5.27c). Inlet feed gas pressure 5 bar and 10 bar have 48% and 62% lesser NO_x emission (ppm) at the outlet of the combustion chamber than the inlet feed gas pressure of 1 bar. The increase in the NO_x concentration (ppm) at the outlet of combustion chamber with an increase in the H_2O concentration in the oxidizer can be seen in Fig. 5.27 (d). The wet oxy-coal combustion

cases having 10-50% H_2O in the oxidizer have 2.5%-75% higher NO_x emission (ppm) at the outlet of combustion chamber than the ideal dry recycle oxy-coal combustion case (0% H_2O in the oxidizer). The oxy-steam combustion case (whole CO_2 is replaced by H_2O in the oxidizer) has 99% higher NO_x emission (ppm) at the outlet of combustion chamber than the ideal dry recycle oxy-coal combustion case.

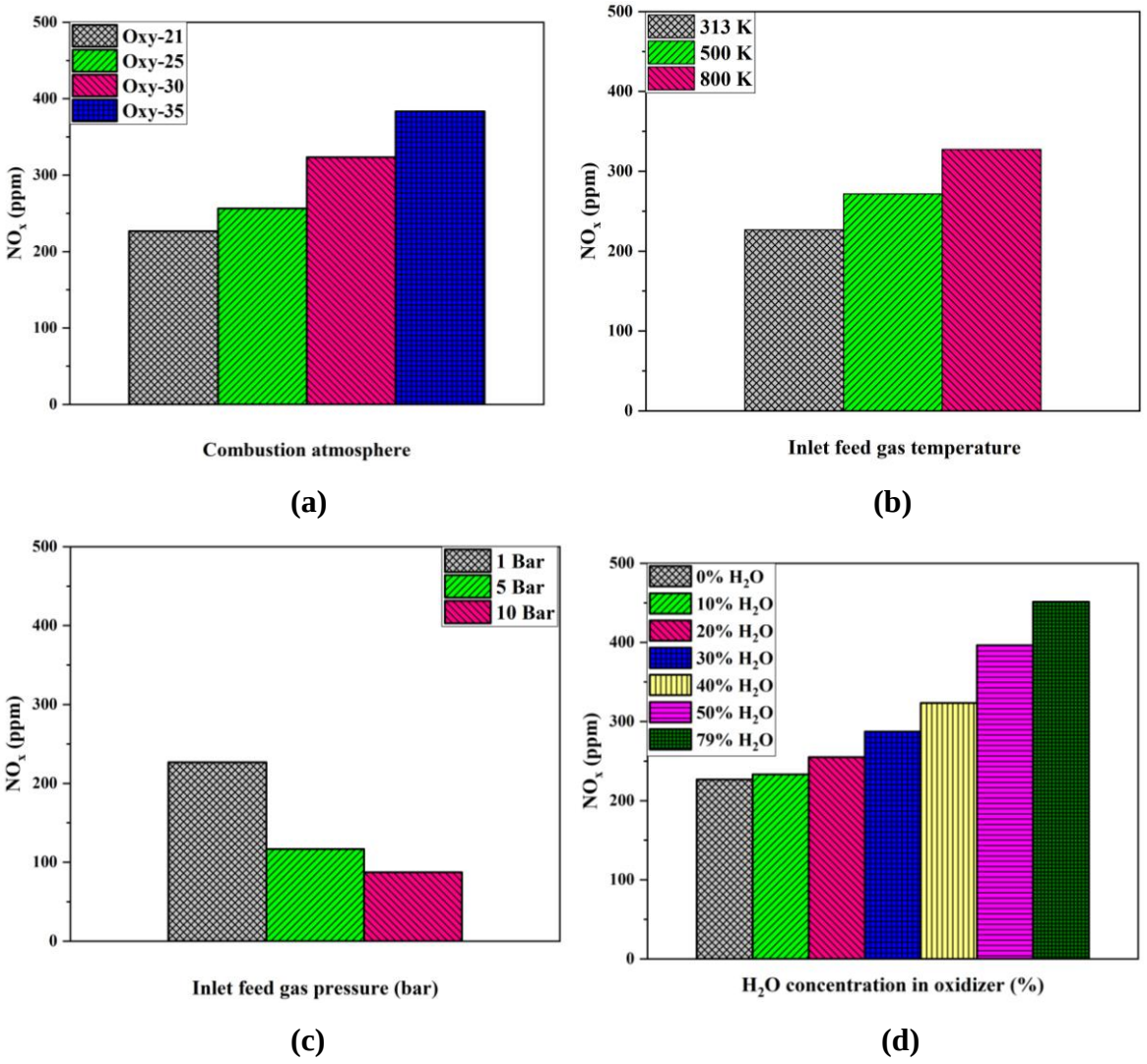

Fig. 5.27. Influence of **(a)** various oxy-coal combustion atmosphere **(b)** inlet temperature of feed gas **(c)** inlet feed gas pressure and **(d)** H_2O concentration in oxidizer on NO_x concentration (ppm) obtained at the outlet of combustion chamber

5.5 Summary

As a closure, this chapter helped in determining the combustion characteristics under oxy-coal (both wet and dry) and oxy-steam combustion atmosphere. Based on the numerical modelling results, it has been found that the predominant influence of lower volume heat capacity of H_2O resulted in an increase in flame temperature as the steam concentration in the oxidizer is increased. The oxy-steam combustion case has produced the highest flame temperature. Enhancement in oxygen consumption has been observed near the burner quarl due to faster oxygen diffusion rate and reduced gaseous volume heat capacity. Based on the discussions held in this chapter, it can be concluded that the influence of char-CO_2 gasification reaction had more a pronounced influence than the char-H_2O gasification reaction on temperature profile and species concentration distribution. This chapter also demonstrated the influence of critical operating parameters such as oxygen concentration, inlet temperature, inlet pressure and H_2O concentration in the oxidizer on the NO_x emission characteristics. Substantial increment in NO_x concentration has been observed with a rise in oxygen concertation in the oxidizer due to enhanced conversion rate of coal_N to NO_x.